*Supplementary Information*

# Operando Raman Spectroscopic Evidence of Electron-phonon Interaction in NiO/$TiO_2$ pn Junction Photodetector

*Wenjun Wang,[a] Zhu Mao,*[a] Yanyu Ren,[a] Fanxu Meng,[b] Xiumin Shi[c] and Bing Zhao*[d]*

[a]School of Chemistry and Life Science, Advanced Institute of Materials Science, Changchun University of Technology, Changchun 130012, China.

[b]Jilin Institute of Chemical Technology, Jilin 132022, China.

[c]College of Chemical Engineering, Changchun University of Technology, Changchun 130012, China.

[d]State Key Laboratory of Supramolecular Structure and Materials, Jilin University, Changchun 130012, China

*To whom correspondence should be addressed.

E-mail: maozhu@ccut.edu.cn (Z. M.) and zhaob@jlu.edu.cn (B. Z.)

# TABLE OF CONTENTS

# EXPERIMENTAL PROCEDURES

## Chemicals

Ammonium fluoride, hydrogen fluoride, and n-butyl titanate were purchased from Macleans Corporation. Ethylene glycol, hydrogen peroxide, and isopropanol were purchased from Tianjin Fuyu Fine Chemical Co., Ltd. (Tianjin, China). Ethanol, hydrochloric acid, acetone, and methanol were purchased from Beijing Chemical Industry Group Co., Ltd. (Beijing, China). These reagents were used without further purification. Ultrapure water was used in the experiments. $NiCl_2$ was purchased from Aladdin and used without further purification.

## Measurements

SEM characterization was performed using a JSM-JEOL 7610F scanning electron microscope with an acceleration voltage of 3.0 kV. The Raman spectra were measured using a Horiba JY LabRAM HR Evolution confocal micro-Raman spectrometer equipped with a multichannel air-cooled charge-coupled device detector. The 532, 633, and 325 nm lasers were used as excitation sources. The Raman spectra measured with the 532 nm excitation were obtained using a 50× objective lens, 3 $mW \cdot cm^{-2}$ laser power (at the samples), and 1800 gr/mm grating. The Raman spectra measured with the 325 nm excitation were obtained using a 15× objective lens, 6.3 $mW \cdot cm^{-2}$ laser power (at the samples), and 1800 gr/mm grating.

## Preparation of TNAs

$TiO_2$ nanotube arrays (TNAs) were prepared on Ti foil using the anodic oxidation method. Ti foil is ultrasonically cleaned in acetone, isopropanol, and methanol solution for 10 min to remove the surface's impurities. Subsequently, the Ti foil was dried under $N_2$ flow. Ti foil was used as the anode, graphite sheet as the cathode, $NH_4F$ glycol

solution and deionized water (0.3% $NH_4F$ + 2% $H_2O$ + 500 mL glycol) as the electrolyte. After electrolysis at 60 V for 3 h, the TNAs were stripped off the Ti foil, washed clean, and $N_2$ dried. Then, it was electrolyzed at 60V for 2h, immersed in ethanol solution for 12 h and calcined at 450 °C for 2 h to obtain Ti foil with TNAs growing on the surface.

**Preparation of NiO modified TNAs**

Ti foil of the prepared TNAs was used as the cathode, graphite sheet as the anode, and 0.01 M $NiCl_2$ aqueous solution as the electrolyte. The TNAs were anodized at 40 V for 20 min, washed with ethanol and deionized water, and calcined at 450 °C for 1 h to form NiO NP-modified TNA (NiO/TNA).

**Preparation of UV Photodetectors (PDs)**

Component A was uniformly formed by mixing 5 mL n-butyl titanate and 9 mL ethanol. Component B was formed by mixing 18 mL ethanol, 1 mL HCl, and 1 mL $H_2O$. Then, component A was added dropwise to component B, and $TiO_2$ sol (light yellow) was obtained after stirring continuously for 4 h.

To prepare the NiO/TNA photodetector (PD), the Ti foil with NiO/TNA film grown on it was oxidized at 60 V for 20 min (the method is the same as the preparation of TNAs). Afterward, the Ti foil was rinsed and immersed in 30% $H_2O_2$ for 10 min to separate the NiO/TNA film from the Ti foil. The NiO/TNA film was rinsed with ethanol and allowed to dry naturally for later use. The $TiO_2$ sol was spread evenly on the Au electrode with $Al_2O_3$ as the substrate, and then transferred to the Au electrode (the NiO/TNA film was perpendicular to the Au interdigital electrode). After that, the Au electrode with the NiO/TNA film adhered was annealed at 450 °C for 2 h to obtain a NiO/TNA photodetector.

# RESULTS AND DISCUSSION

## Calculation of responsivity and detection rate for PDs

To further evaluate the photoelectric performance of the three devices, the following formula was used to calculate the responsivity of the PDs:

$$R = \Delta I/PS,$$

where $\Delta I = I_{ph} - I_d$, $V_{bias} = 3$ V, $P = 6.2$ mW·cm$^{-2}$; I is the intensity of the incident laser, and $S = 5.027 \times 10^{-7}$ cm$^2$ is the effective area under illumination. Under 325 nm laser illumination, the responsivity of M-NiO/TNA PD was calculated to be 19.28 A·W$^{-1}$. Similarly, the detection rate (D*), an index for evaluating the photoresponse characteristics of a PD, can be described as follows:

$$D^* = R/(2qI_{dark}/ S)^{1/2},$$

where $I_{dark}$ is the dark current, and q refers to the absolute value of the electron charge ($1.6 \times 10^{-19}$ C). The D* of the M-NiO/TNA PD was calculated to be $2.31 \times 10^9$ Jones. This small D* value was mainly due to the large dark current.

It should be noted that the R and D* of M-NiO/TNA PD are 14 and 4 times that of the TNA PD, and 38 and 10 times that of L-NiO/TNA PD, respectively. An internal electric field is generated at the interface area of the pn junction, which is more conducive to the separation of photogenerated carriers, which ultimately improves the photoelectric performance of the M-NiO/TNA PD.

## Time response behavior of PDs

As shown in Figure 3j, the photocurrents ($I_{ph}$) of the M-NiO/TNA, L-NiO/TNA, and TNA PDs are 1087, 33, and 74 nA, respectively. Their dark currents ($I_d$) are 154, 11, and 15 nA, respectively. Additionally, for the M-NiO/TNA PD, the on/off ratio of the current signal is 7, which is significantly higher than those of 3 and 5 obtained for L-NiO/TNA and TNA, respectively. It is worth noting that among the three devices,

the photoelectric performance of L-NiO/TNA PD is the worst, while the M-NiO/TNA is the best, which may be due to the following reasons: 1) When preparing L-NiO/TNA, the higher temperature of the electrolyte (approximately 30 °C) causes damage to the structure of TNA and introduces defects. Photogenerated carriers are easily captured by these defects, resulting in reduced photoelectric detection performance and delayed response. 2) In L-NiO/TNA, owing to the low content of NiO NPs, there is no effective pn heterojunction formation because the interface area formed is too small. In contrast, the introduced grain boundary defects easily cause recombination of the photogenerated carriers. Therefore, the TNA PD has a better light responsivity without grain boundary defects. Moreover, the increase in the interface area of the pn heterojunction formed by M-NiO/TNA is sufficient to achieve a rectifying effect, which is conducive to the separation of carriers at the interface, thereby reducing the probability of recombination. 3) The NiO content in L-NiO/TNA was less and the distribution was more dispersed, while the NiO NPs in M-NiO/TNA aggregated into clusters with higher surface scattering, which promoted the collection of photocurrent at the NiO/TNA interfaces; the increase in the interface area of the pn heterojunction between the high content of NiO particles and TNA is conducive to separating the doped carriers at the interface and reducing the recombination probability, thereby improving the photoelectric performance of the NiO/TNA heterojunction.

**Stability of PDs**

To further evaluate the stability of the devices, the three PDs (M-NiO/TNA, L-NiO/TNA, and TNA PDs) were placed in the dark for 100 days before measuring their photoelectric performance (Figure 3k). The results show that under long-term UV laser illumination (open time of 120 s, close time of 60 s), the photocurrents of M-NiO/TNA, TNA, and L-NiO/TNA PDs rapidly rise to stable values of 1000, 125, and 36 nA, respectively. The photocurrent decreased rapidly and returned to its initial state after the UV laser turn off. Three PDs can easily switch between the "on" and

"off" states within five cycles, indicating that the photocurrent signal response is consistent and repeatable. These results indicate that a large number of p-NiO/n-TNA interfaces (pn junctions) is beneficial for improving the performance of TNA PDs. After 100 days in the dark, the photocurrents of the three PDs did not decrease significantly compared with the photocurrent obtained from the initial test. This proves that the prepared PDs have excellent stability and can be recycled repeatedly.

**Laser response speed of PDs**

As shown in Figure 3l, laser response speed is another important quality factor in PD. The rise time ($\tau_r$) and fall time ($\tau_d$) are defined by the rising interval of the photocurrent signal when the laser is turned on (from 10% to 90% of the maximum photocurrent) and the fall interval of the photocurrent when the laser is turned off (90–10% of the maximum photocurrent).

As shown in Table 1, compared to the p-NiO/n-$TiO_2$ PDs prepared by other researchers ($\tau_r$ = 300 s and $\tau_d$ = 400 s)[1], the response speed of the M-NiO/TNA PDs prepared in this work is significantly improved.

## FIGURES S1 AND S2

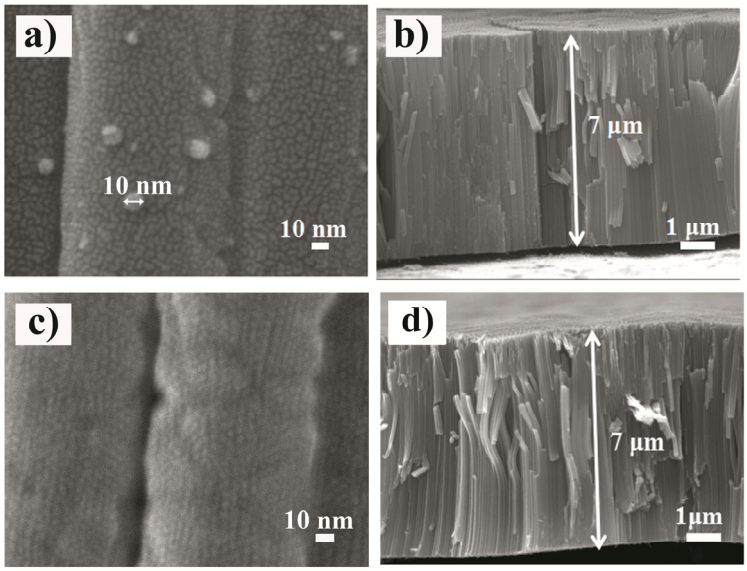


**Figure S1.** High-resolution SEM images of side-view (400,000×) of a) NiO/TNA and c) TNA; Side-view SEM images of b) NiO/TNA and d) TNA.

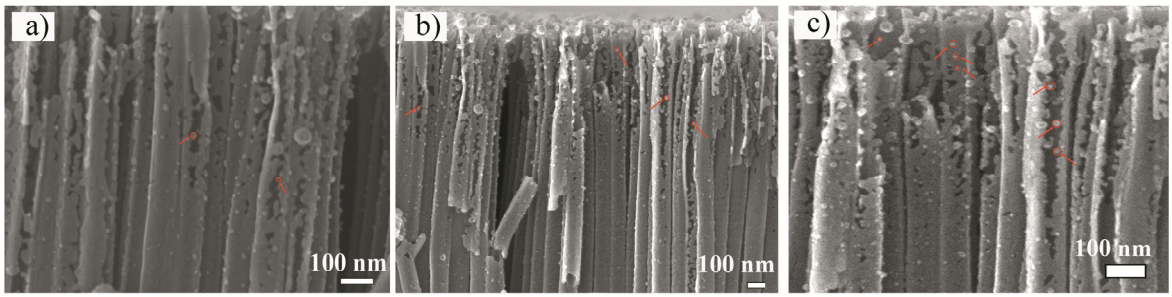


**Figure S2.** SEM images of cross-sectional view of NiO/TNA.

By controlling the preparation temperature, the amount of NiO NPs modified on the TNAs can be adjusted, realizing the performance adjustment of the PDs. The average diameter of the $TiO_2$ nanotubes (TNA) was approximately 70 nm. It can be seen clearly that the average diameter of the NiO NPs is approximately 10 nm. The results show that the modification of NiO NPs did not change the tube length of the TNA (~7 µm).

## FIGURE S3

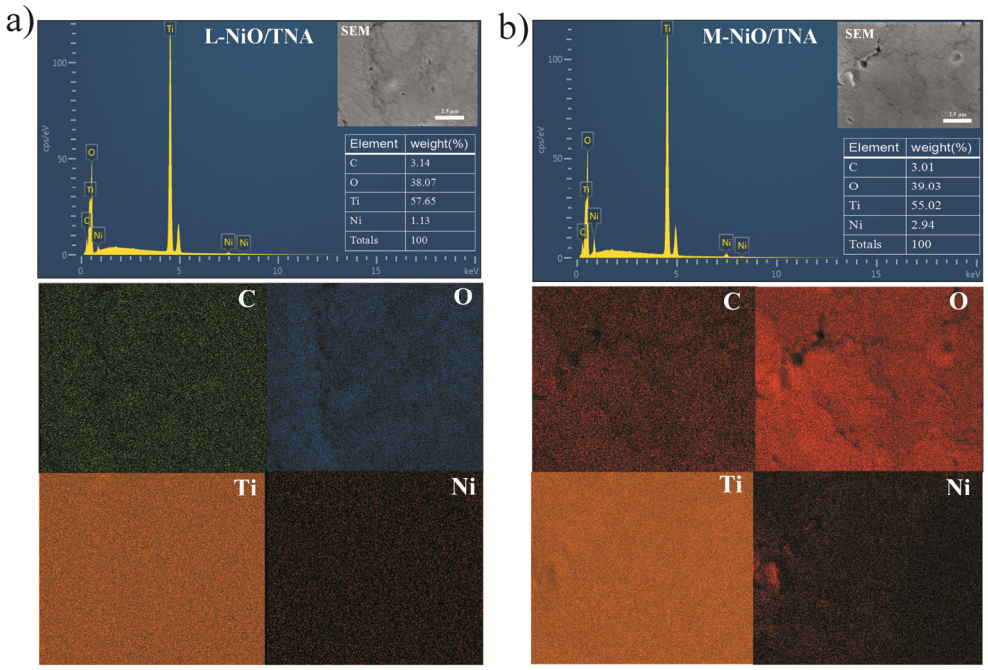


**Figure S3**. Energy dispersive spectroscopy (EDS) spectra and elemental mapping images of a) L-NiO/TNA and b) M-NiO/TNA, showing the distribution of chemical elements (C, O, Ti, and Ni).

**FIGURE S4**

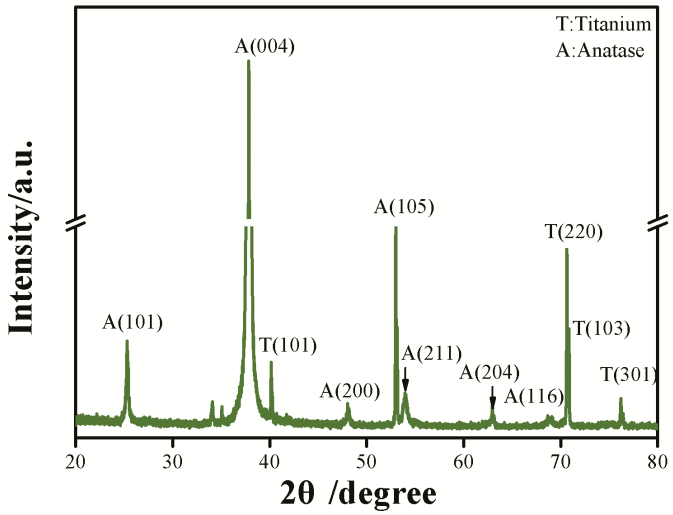


**Figure S4.** XRD patterns of TNAs.

## FIGURE S5

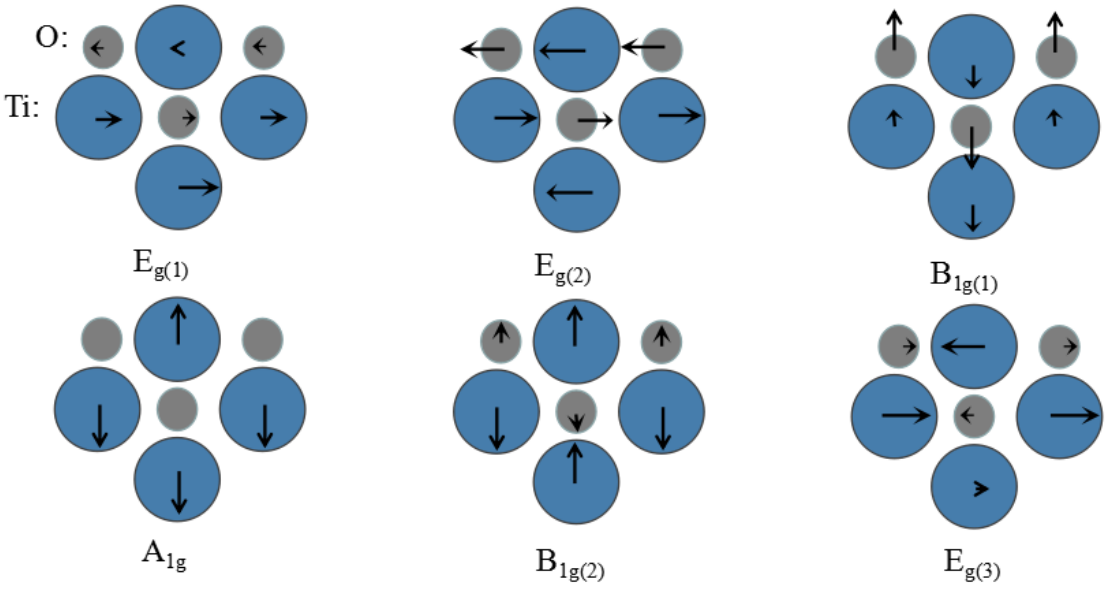


**Figure S5.** Vibration modes of six phonon modes in anatase $TiO_2$.

## FIGURE S6

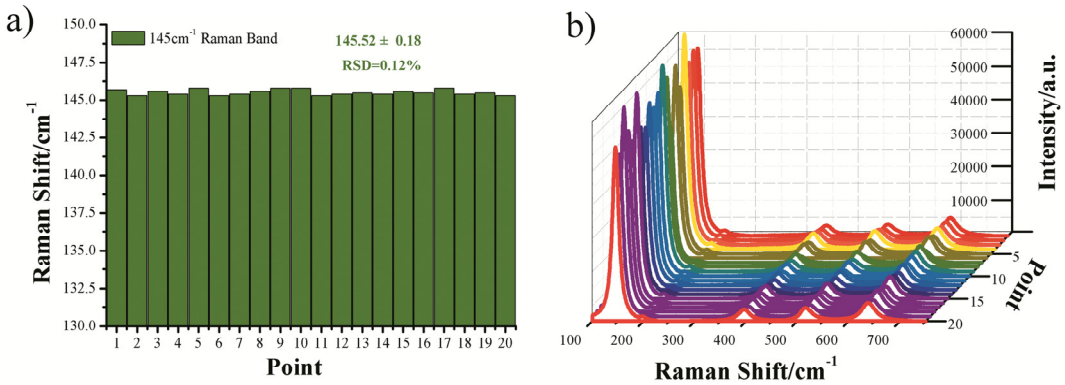


**Figure S6.** The 145cm$^{-1}$ band of TNA-PD: a) RSD of Raman shift, b) Raman spectra. These bands are obtained from 20 sets of randomly selected data. RSD is the relative standard deviation.

We have provided 20 sets of Raman spectroscopy data for testing TNA photodetectors under 325 nm laser irradiation, indicating that the band position of $E_{g(1)}$ as a sensitive marker is concentrated near 145 cm$^{-1}$ (Figure S6). As shown in Figure S6a, when the 145cm$^{-1}$ band is selected for RSD calculation, the RSD of the Raman shift is 0.12%. Figure S6b shows the full Raman spectra of the 20 sets of Raman data in Figure S6a. Therefore, operando Raman spectroscopy shows stable repeatability. That is, in the absence of NiO/$TiO_2$ pn junciton, the $E_{g(1)}$ band position has very high stability and repeatability. This result also proves that the existence of NiO/$TiO_2$ pn junciton causes phonon shifts of TNA. Moreover, the shifts of NiO/TNA relative to TNA support the interaction of electrons and phonons on the pn junction of NiO/TNA.

## FIGURE S7

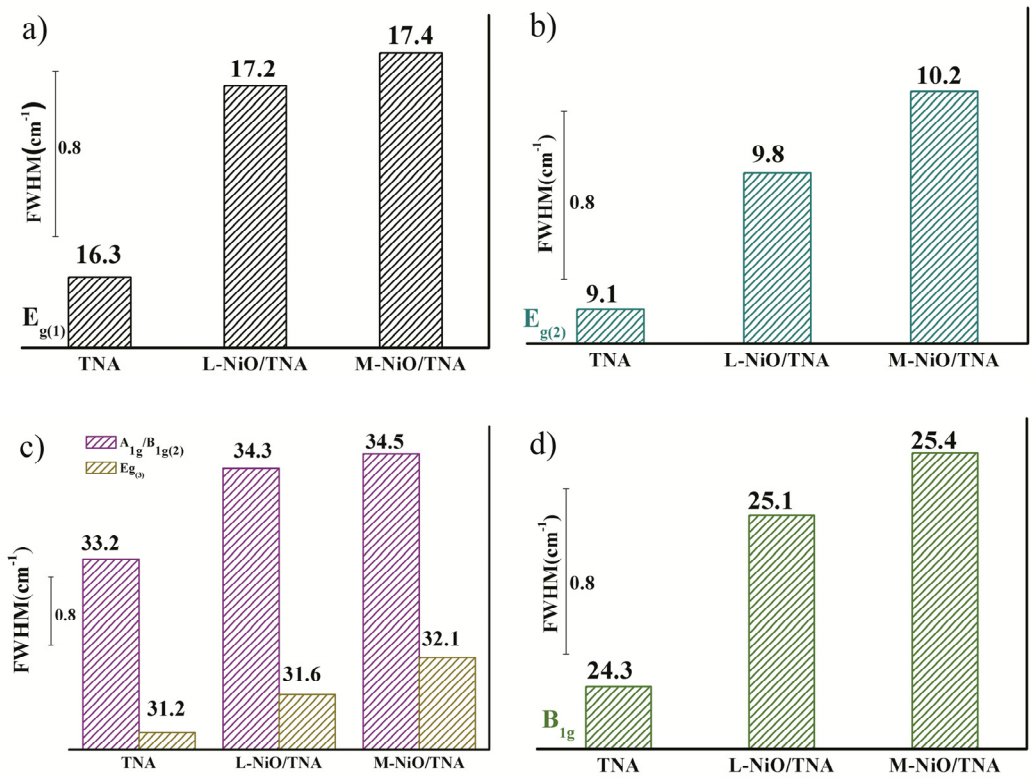


**Figure S7.** The FWHM of the phonon modes of the three PDs, a) $E_{g(1)}$, b) $E_{g(2)}$, c) $A_{1g}/B_{1g(2)}$ and $E_{g(3)}$, and d) $B_{1g}$.

## FIGURE S8

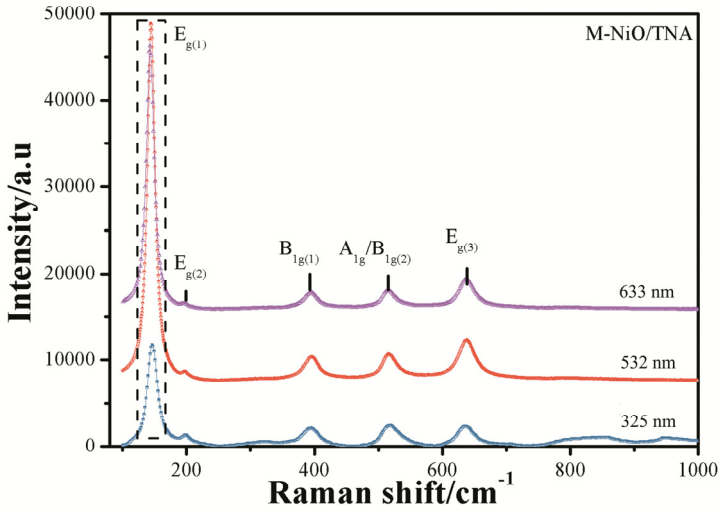


**Figure S8.** Raman spectra of M-NiO/TNA PD irradiated by 325, 532, and 633 nm lasers.

## FIGURE S9

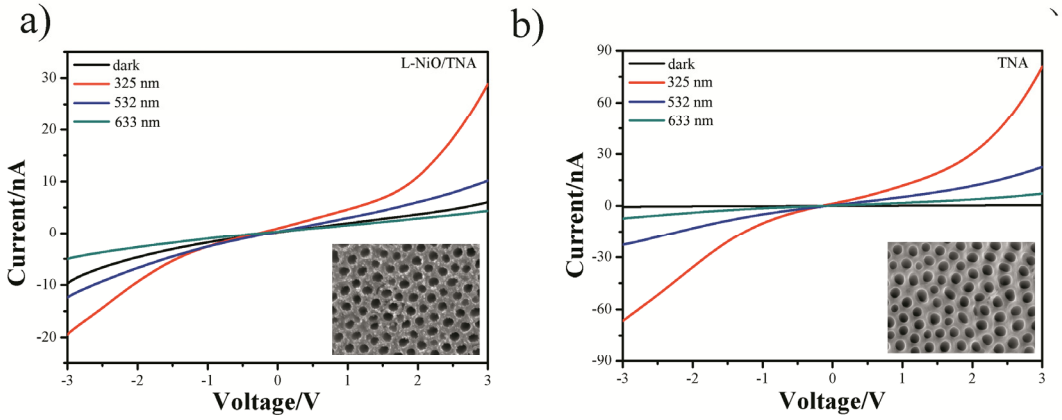


**Figure S9.** I-V curves of a) L-NiO/TNA PD and b) TNA PD, respectively.

According to Figures 4, and S9, it is found that the three PDs show measurable and large current signals at zero bias under darkness and three laser illuminations, indicating that they all have self-powered capability. Figures 4a-c show that the symmetry of the I-V curve of M-NiO/TNA PD (compared with TNA PD) was better than that of the other two PDs (L-NiO/TNA PD and TNA PD), showing the smallest offset. This is because the self-powered M-NiO/TNA PD is the result of the Schottky junction formed by $TiO_2$ nanotubes and gold electrodes and the pn heterojunction formed by $TiO_2$ nanotubes and NiO NPs, which counteract the reverse current. In general, Schottky contacts provide a greater reverse current than pn junctions.

## FIGURE S10

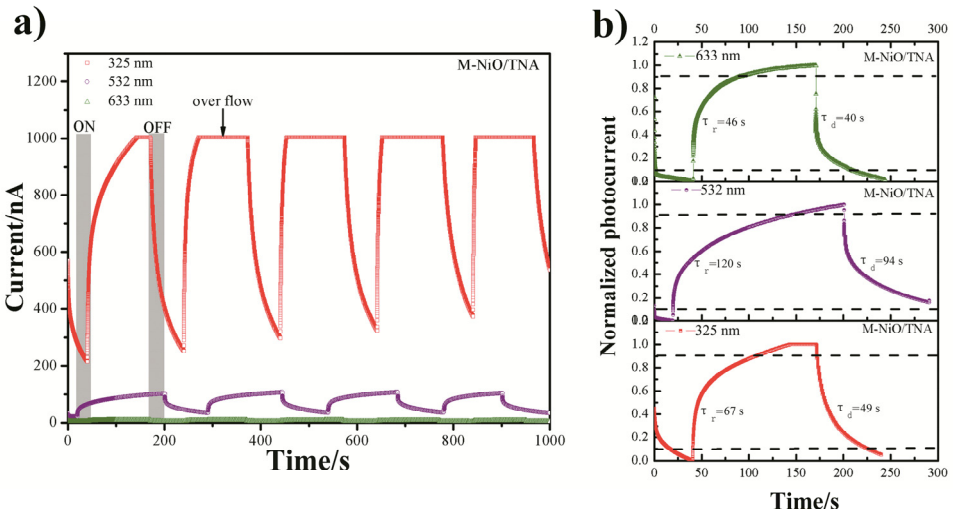


**Figure S10.** M-NiO/TNA PD a) Time response behavior of 5 consecutive cycles of "on" and "off" under a 3 V bias with three laser illuminations. b) Normalized photocurrent-time curve under 325, 532, and 633 nm lasers.

As shown in Figure S10a, M-NiO/TNA PD is in the "on" and "off" states five times under 325, 532, and 633 nm Raman lasers, and the photocurrent of the device does not decrease, indicating that M-NiO/TNA PD shows good cyclability and stability under these three lasers. Figure S10b shows that under a 325 nm UV laser, the $\tau_r$ and $\tau_d$ values of M-NiO/TNA PD are 67 and 49 s, respectively. Under 532 nm and 633 nm visible lasers, the ($\tau_r$ and $\tau_d$) values were (120 s, 46 s) and (94 s, 40 s), respectively. This result indicates that M-NiO/TNA PD has the fastest response under 633 nm laser illumination.

# REFERENCE

1. S. Pansri, R. Supruangnet, H. Nakajima, S. Rattanasuporn and S. Noothongkaew, *Journal of Materials Science*, 2019, **55**, 4332-4344.